



CrossMark
click for updates

Cite this: *RSC Adv.*, 2016, 6, 25034

A cobalt Schiff base complex on TiO₂ nanoparticles as an effective synergistic nanocatalyst for aerobic C–H oxidation

Maasoumeh Jafarpour,* Hossein Kargar and Abdolreza Rezaeifard*

A novel visible light active TiO₂ nanoparticle was produced by functionalization with a cobalt Schiff base complex under ultrasonic agitation. It was characterized by different techniques such as FT-IR, EDX, XPS, ICP-AES and TGA. The particle size of the synthesized nanocomposite was found to be in the range of 22–32 nm according to TEM images. A red-shift of the band-edge and a significant reduction of the band-gap (2.9 eV) were revealed by UV-DRS. The as-prepared nanocomposite demonstrated high oxidation activity and desired selectivity in the aerobic benzylic C–H oxidation of a structurally diverse set of alcohols and benzylic hydrocarbons. A synergistic effect of the cobalt Schiff base complex and TiO₂ nanoparticles on the visible-light photocatalytic activity was explored. Spectral results and leaching experiments revealed that the heterogeneous catalyst preserved its structure after many reuses.

Received 23rd December 2015
Accepted 27th February 2016

DOI: 10.1039/c5ra27520b

www.rsc.org/advances

1. Introduction

Aerobic oxidation mediated by heterogeneous catalysts is an attractive and challenging transformation from a chemical and industrial points of view.¹ Different transition metal-based systems have been successfully used for the aerobic C–H oxidation producing invaluable oxygen containing compounds as versatile intermediates. In this regard, several challenges exist, such as the need of low pressures of O₂ especially in flammable organic solvents, mild reaction conditions, low catalyst loadings, and the avoidance of costly or toxic additives. Another main issue is the chemoselectivity of the method to achieve desired transformations when other groups susceptible to oxidation are present.²

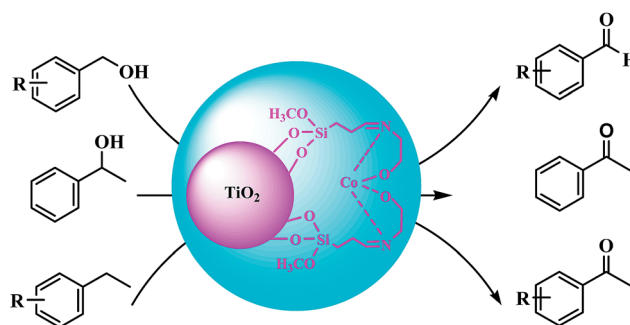
Photocatalytic oxidation with O₂ has been studied extensively with semiconductor materials such as titanium dioxide.^{3–7} One of the most critical issues for practical application of photocatalytic processes is the low catalytic activity under visible light irradiation ($\lambda > 400$ nm), the main component of solar irradiance. To date, many strategies have been utilized to improve the photocatalytic performance of TiO₂, including nano sizing,^{8–10} metal-ion doping,¹¹ anion doping,^{12,13} noble metal loading^{14–16} and dye sensitization,^{17,18} which are easy to be realized. Self-assembly,^{19,20} biotemplating^{21,22} and surfactant templating²³ are further developments in this line. However, design and fabrication of novel visible-light-driven catalysts that promote the efficiency of aerobic oxidations is still a challenge

in modern catalytic science.²⁴ In this line of research, herein, we wish to develop a new visible light photocatalyst by surface modification of nanocrystalline TiO₂ with cobalt Schiff base complex. The catalyst demonstrated high efficiency and desired selectivity towards aerobic benzylic C–H oxidation of alcohols and hydrocarbons in acetonitrile (Scheme 1). The additional advantage of this catalytic system is facile and efficient reusability of the solid catalyst.

2. Experimental

2.1. General remarks

All chemicals were purchased from Merck and Fluka Chemical Companies. Powder X-ray diffraction (XRD) was performed on a Bruker D8-advance X-ray diffractometer with Cu K α ($\lambda = 1.54178$ Å) radiation. The FT-IR spectra were recorded on



Scheme 1 Aerobic benzylic C–H oxidation catalyzed by CoL₂@TiO₂ nanocomposite.

Catalysis Research Laboratory, Department of Chemistry, Faculty of Science, University of Birjand, Birjand, 97179-414 Iran. E-mail: mjafarpour@birjand.ac.ir; rrezaeifard@birjand.ac.ir; rrezaeifard@gmail.com; Fax: +98 561 2502515; Tel: +98 561 2502516

NICOLET system. Thermogravimetric analysis (TGA) of nano powders was performed in air by Shimadzu 50. TEM images were obtained by TEM instrumentation 906E (Zeiss, Jena, Germany). Sample for TEM experiment was prepared by dispersing the samples in ethanol, sonicating for 30 min to ensure adequate dispersion of the nanostructures, and evaporating one drop of the solution onto a 200 mesh form bar-coated copper grids. XP spectra were recorded using a BES-TEC GMBH (10^{-10} mw) with Al anode. Diffuse reflectance UV-Vis spectra were recorded using an Avantes spectrometer (Avaspec-2048-TEC model). Progresses of the reactions were monitored by TLC using silica-gel SIL G/UV 254 plates and also by GC-FID on a Shimadzu GC-16A instrument using a 25 m CBP1-25 (0.32 mm ID, 0.5 μ m coating) capillary column. NMR spectra were recorded on a Bruker Avance DPX 400 MHz instruments.

2.2. The preparation of organosilicon aldehyde

To a solution of (3-chloropropyl) trimethoxysilan (0.74 mL, 4 mmol) in DMSO (0.35 mL, 5 mmol) was added NaHCO_3 (0.67 g, 8 mmol). The solution was refluxed at 155 $^\circ\text{C}$ for 2 h. Then, water (50 mL) was added to the reaction mixture and the product extracted with Et_2O (2×50 mL). The organic layer was separated and dried over anhydrous CaCl_2 and filtered. Evaporation of the solvent afforded the desired product (yellow oil, 70% isolated yield). Structural assignments of the product is based on their FT-IR, ^1H NMR.²⁵

2.3. The preparation of Schiff base ligand

To a solution of (3-oxopropyl) trimethoxysilan (0.8 mL, 5 mmol) in ethanol (10 mL) was gradually added a solution of ethanol amine (0.3 mL, 5 mmol) in ethanol (10 mL) at 60 $^\circ\text{C}$ under ultrasonic agitation. Then, the reaction mixture remained under the same conditions for 60 min. Afterwards, the product which was precipitated after 24 hours at room temperature, filtered and washed with ethanol and dried in desiccators. (85% isolated yield) structural assignments of the product is based on their FTIR, ^1H NMR.²⁵

2.4. The preparation of Co(II) Schiff base complex

A solution of cobalt acetate (0.44 g, 2.5 mmol) in ethanol (10 mL) was added to a solution of Schiff base ligand (5 mmol, 0.25 g) in 10 mL ethanol at 60 $^\circ\text{C}$ under ultrasonic agitation. Then, the reaction mixture remained under the same conditions for 3 hours. The complex which was precipitated after cooling the reaction mixture, filtered and washed with cold ethanol. Finally, Co(II) Schiff base complex was obtained after drying at 100 $^\circ\text{C}$ under vacuum. (92% isolated yield). Structural assignments of the product is based on their FTIR, ^1H NMR.²⁵

2.5. Fabrication of TiO_2 nanoparticles

To a solution of TiCl_3 (0.05 mol) in a mixture of double-distilled water and absolute ethanol (1 : 1) was added citric acid (0.15

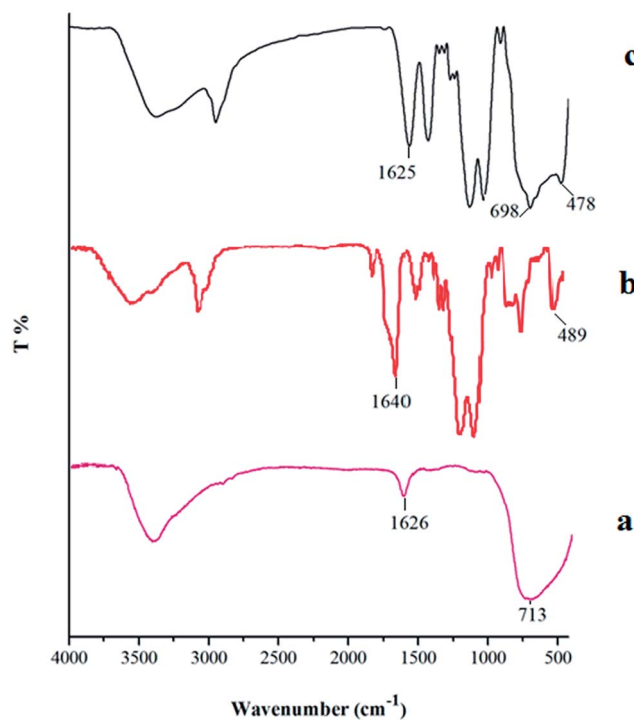
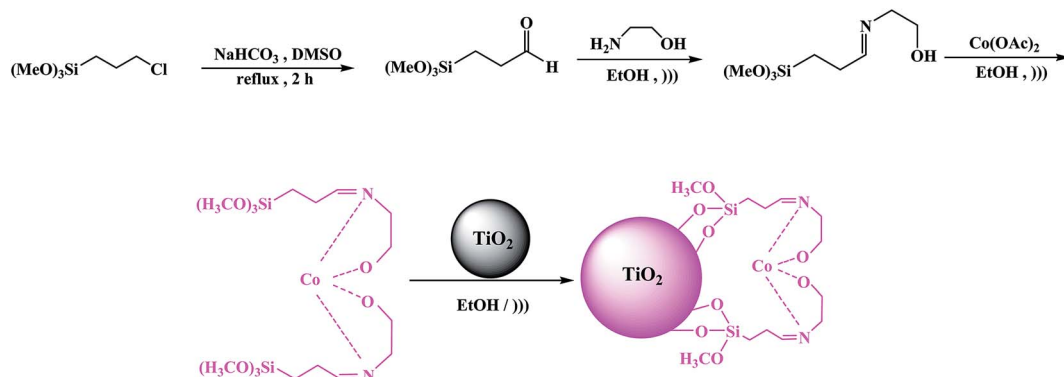


Fig. 1 FT-IR spectra of (a) TiO_2 nanoparticles, (b) Co(II) Schiff base complex and (c) $\text{CoL}_2@ \text{TiO}_2$.



Scheme 2 Preparation of $\text{CoL}_2@ \text{TiO}_2$ nanocomposite.

mol) and ethylene glycol (0.15 mol) subsequently. The resulting mixture was dissolved at 45 °C under ultrasound for 15 min to give a clear violet solution. The solution was refluxed at 120 °C

for 8 h which turned into a metal–citrate homogeneous complex with a little color change from clear violet to black-violet. After cooling down, in order to bring about the required chemical

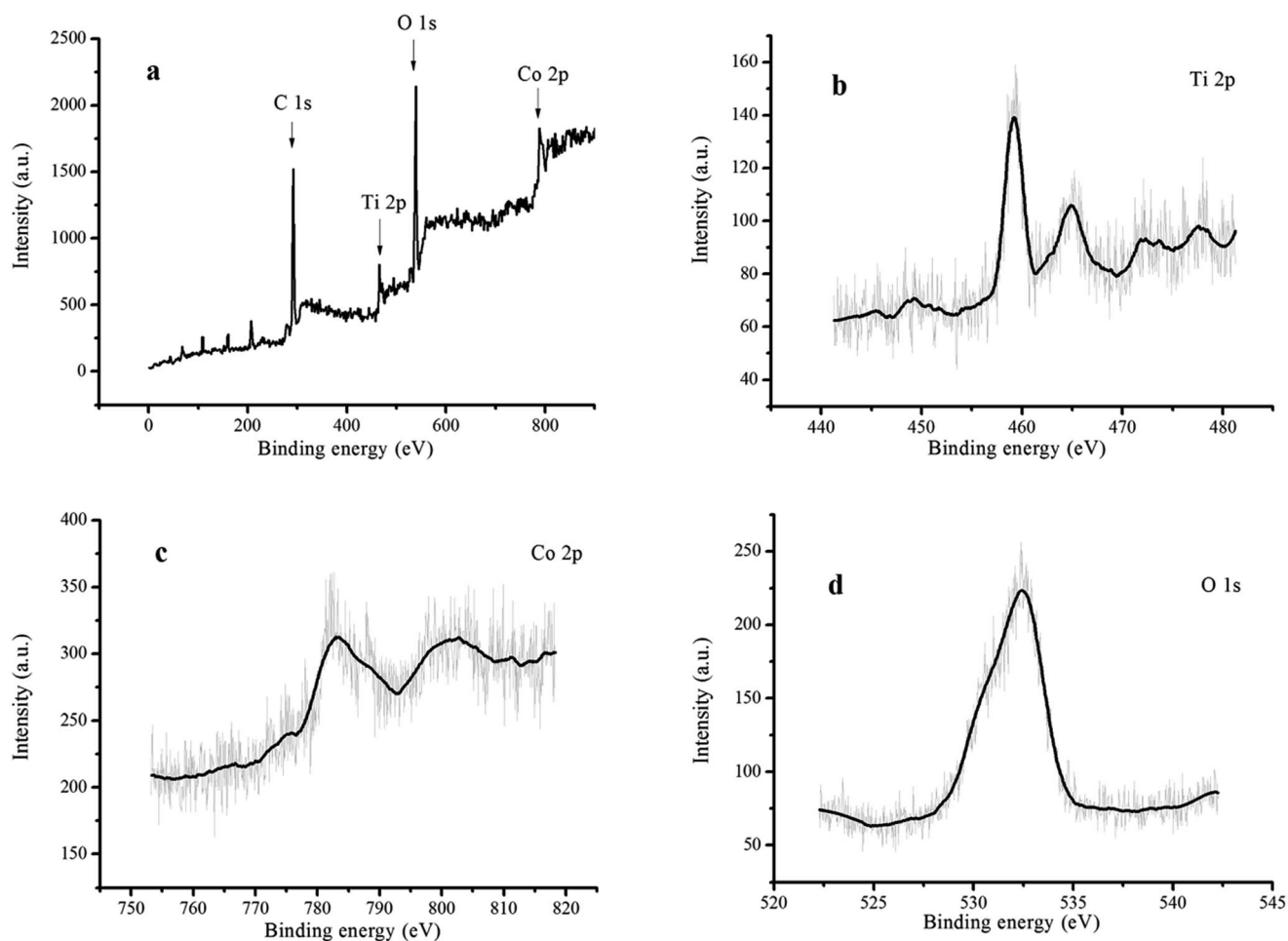


Fig. 2 XPS spectra of $\text{CoL}_2@ \text{TiO}_2$ nanocomposite (a) wide scan, (b) Ti 2p, (c) Co 2p, and (d) O 1s.

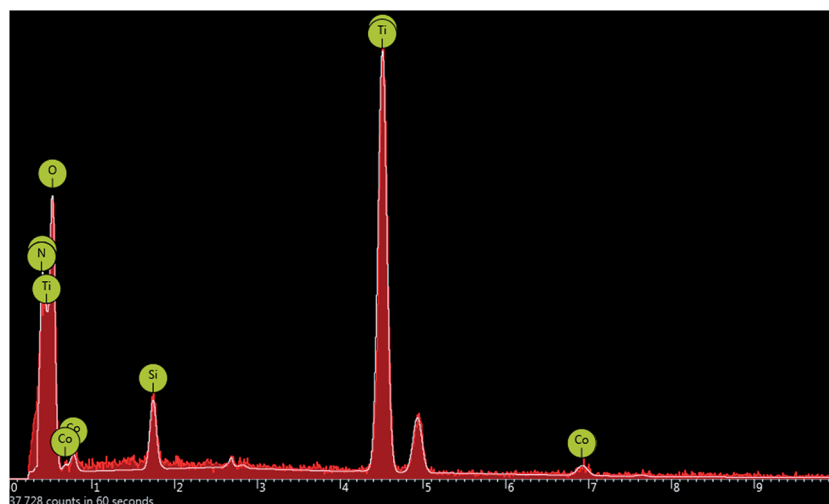


Fig. 3 EDX analysis of $\text{TiO}_2/ \text{CoL}_2$ nanocomposite.

reactions for the development of polymerization and evaporation of the solvent, the sol was further slowly heated at 90 °C for 6 h in an open bath until a beige wet gel was obtained. During continuous heating at this temperature, the polymerization between citric acid, ethylene glycol and complexes is developed and ultimately sol became more viscous as a wet gel. In the final step of sol-gel process, the wet gel was fully dried by direct heating on the hot plate at 150 °C for 6 h. The resultant production was a black powder. Then it was calcined in a furnace at 600 °C for 3 h at a rate of 5 °C min⁻¹. Finally TiO₂ nanoparticles with a white color were obtained.²⁶

2.6. Preparation of TiO₂/CoL₂ nanocomposite

To 1.0 g of TiO₂ nanoparticles was gradually added 1.0 g CoL₂ in ethanol over a period of 60 min at 60 °C under ultrasonic agitation. Then, the as-obtained mixture was refluxed for 6 h. Afterwards, the product was centrifuged and washed by ethanol. Finally, CoL₂@TiO₂ nanocomposite was obtained after drying for 3 h at 70 °C.

2.7. General procedure for aerobic oxidation of benzyl alcohols

To a mixture of benzyl alcohol (1 mmol) and TiO₂/CoL₂ nanocomposite (0.5 mol%) in CH₃CN (2 mL) was added NHPI (10 mol%, 0.016 g) and the reaction mixture was stirred under 1 atm. O₂ (7–10 mL min⁻¹) and visible light at 70 °C for the required time. The reaction progress was monitored by GC, and the yields of the products were determined by GC and NMR analysis.

2.8. General procedure for aerobic oxidation of alkyl benzenes

To a mixture of alkyl benzene (1 mmol) and TiO₂/CoL₂ nanocomposite (0.75 mol%) in CH₃CN (2 mL) was added NHPI (10 mol%, 0.016 g) and the reaction mixture was stirred under 1 atm. O₂ (7–10 mL min⁻¹) and visible light at 70 °C for the required time. The reaction progress was monitored by GC, and the yields of the products were determined by GC and NMR analysis.

2.9. Reusability of catalyst

To a mixture of 1-phenyl ethanol (1 mmol) and TiO₂/CoL₂ nanocomposite (0.5 mol%) in CH₃CN (2 mL) was added NHPI (10 mol%, 0.016 g) and the reaction mixture was stirred under 1 atm. O₂ (7–10 mL min⁻¹) and visible light at 70 °C for 3 h. After completion of the reaction, TiO₂/CoL₂ nanocomposite was separated by centrifuging followed by decantation (3 × 5 mL ethylacetate). The isolated solid phase (TiO₂/CoL₂ nanocomposite) was dried under reduced pressure and reused for next runs. Catalyst recovery was also investigated in the aerobic oxidation of alkyl benzenes in acetonitrile according to the above mentioned procedure.

3. Results and discussion

3.1. Synthesis and characterization of catalyst

As shown in Scheme 2, organosilicon aldehyde prepared by oxidation of (3-chloropropyl) trimethoxysilane was used as an appropriate linker for a new heterogeneous supported catalyst. Condensation with ethanolamine gave a new Schiff base.²⁵ The Co Schiff base complex was prepared (CoL₂) by condensation of the Schiff base (HL) with Co(OAc)₂. It was then immobilized on TiO₂ nanoparticles of approximately 18–20 nm diameters²⁶ for improving the visible light photocatalytic properties of nanocrystalline TiO₂ (Scheme 2).

The FT-IR spectra of TiO₂ nanoparticles, Co(II) Schiff base complex and CoL₂@TiO₂ nanocomposite, have been depicted in Fig. 1. Significant spectral changes support the formation of the respective composite. The major band at 1625 cm⁻¹ is attributed to imine bond as well as remaining hydroxyl groups on TiO₂ surface. A strong peak at 1131 cm⁻¹ corresponds to the Si–O bond. Major bands at 500–750 cm⁻¹ are related to the stretching vibrations of Ti–O group and a weak band at 478 cm⁻¹, which corresponds to the Co–N bond.

XPS was applied to detect elements containing nanocomposite and their oxidation states. According to the spectra in Fig. 2, the C 1s core level peak at 285 eV of binding energy was

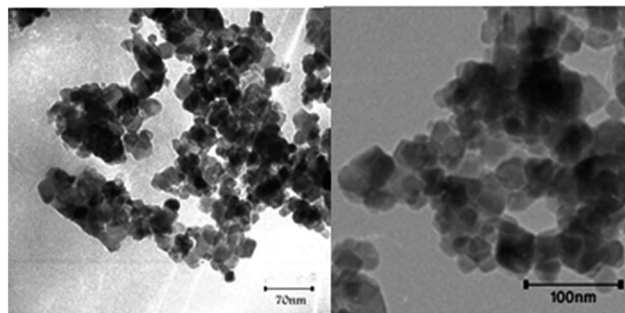


Fig. 4 TEM images of TiO₂ (left) and CoL₂@TiO₂ nanocomposite (right).

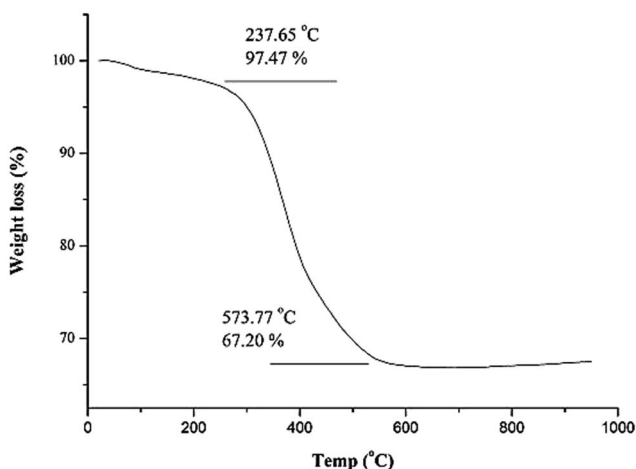


Fig. 5 The TGA of CoL₂@TiO₂ nanocomposite.

taken as the reference. The respective peaks for Ti 2p, Co 2p and O 1s confirm the presence of these elements in the nanocomposite (Fig. 2a). The high resolution narrow-scan XPS spectra of Ti 2p and Co 2p and O 1s peaks of the sample are shown in Fig. 2b–d, respectively. Two intense bands located at 459 and 465 eV binding energy represent the Ti $^{2}P_{3/2}$ and Ti $^{2}P_{1/2}$, respectively. Also the peak of Co $^{2}P_{3/2}$ located at ~ 782.92 eV and that of Co $^{2}P_{1/2}$ at ~ 801 eV, verify that cobalt was mainly present in the II oxidation state.^{27–29} The binding energy at 532 eV is attributed to the contribution of oxygen (O 1s).^{27–30}

The presence of Co atoms in nanocatalyst was also confirmed by the EDX spectroscopy analysis as shown in Fig. 3. The other peaks have been clearly observed from the spectrum, which are identified as Ti, Si, O and N.

Transmission electron microscopy (TEM) clearly revealed spherical morphology for TiO₂ and CoL₂@TiO₂ nanocomposite

with size ranging between 18–20 nm and 22–32, respectively (Fig. 4).

The TGA curve of CoL₂@TiO₂ nanocomposite (Fig. 5) demonstrates its thermostability up to 237 °C. The organic parts decomposed completely at 573 °C. From the TGA, the amount of Co was evaluated to be 3.2 wt%, which is in good agreement with the value determined by inductively coupled plasma atomic emission spectroscopy (ICP-AES; 3.08%).

3.2. The catalytic activity of TiO₂/CoL₂ nanocomposite

The CoL₂@TiO₂ nanocomposite was initially investigated for the oxidation of 1-phenyl ethanol with O₂ (1 atm) in acetonitrile (2 mL), as this did not proceed in the absence of the catalyst under any conditions. The reaction conditions optimized with respect to different factors such as solvent nature,

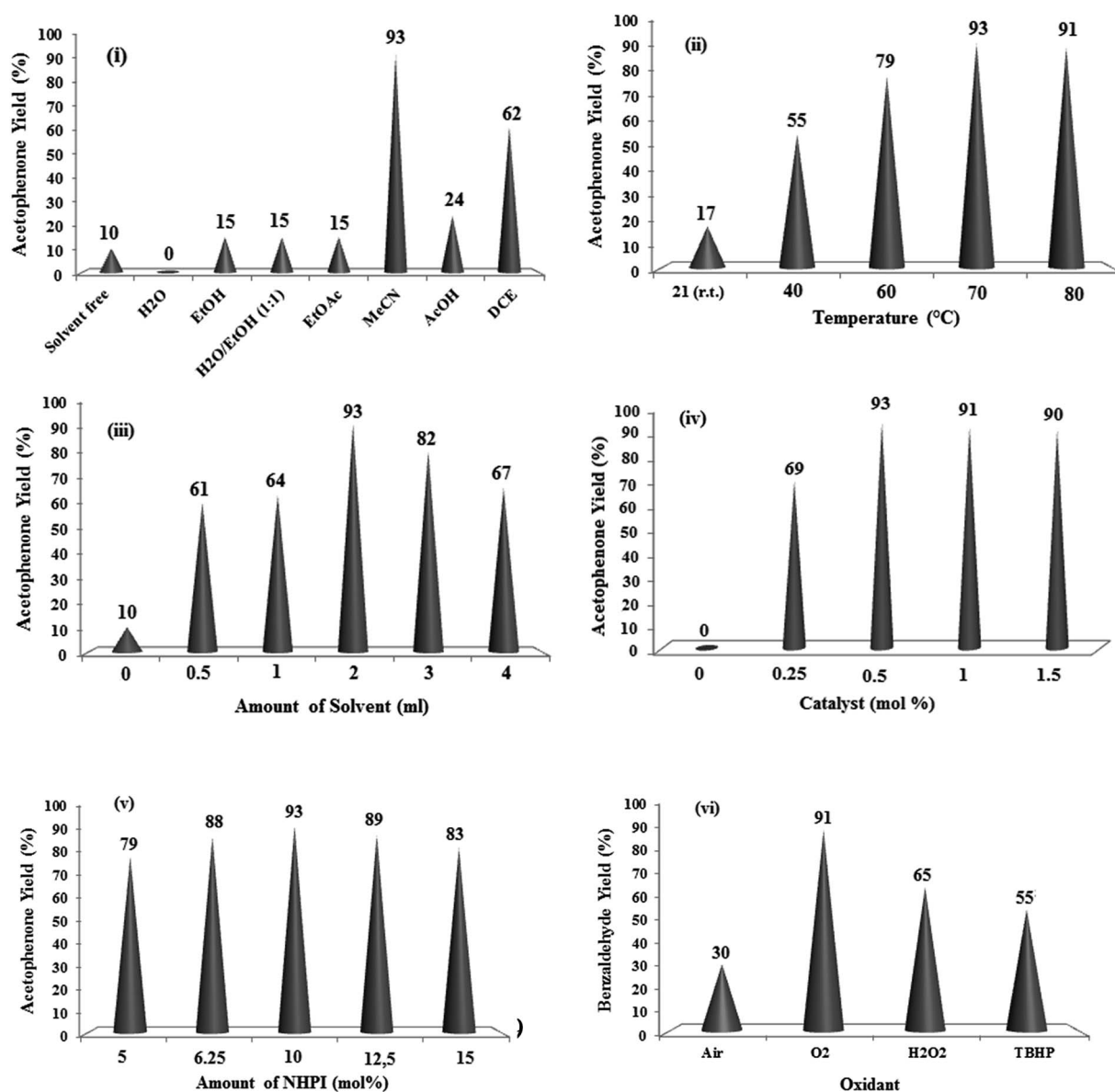


Fig. 6 The screening of the (i) solvent nature (ii) temperature (iii) solvent amount (iv) catalyst amount (v) NHPI amount and (vi) oxidant nature on the oxidation of 1-phenyl ethanol (1 mmol) catalyzed by CoL₂@TiO₂ after 3 h.

Table 1 Oxidation of benzylic alcohols using NHPI/O₂ oxidative system catalyzed by CoL₂@TiO₂ nanocomposite^a

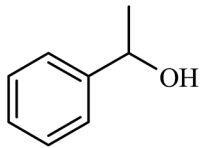
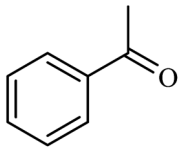
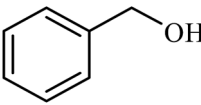
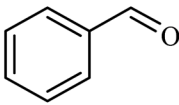
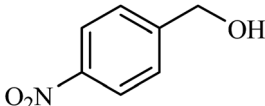
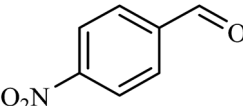
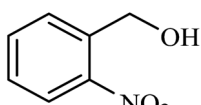
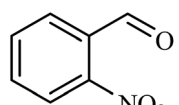
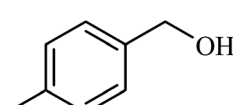
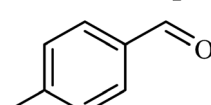
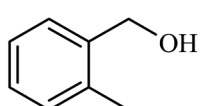
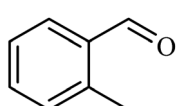
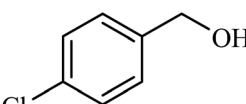
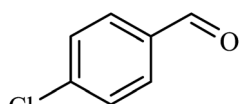
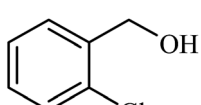
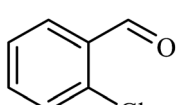
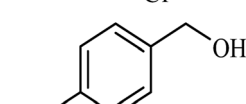
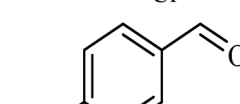
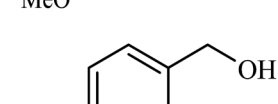
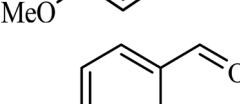
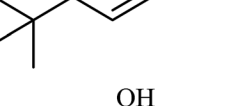
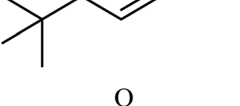
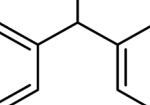
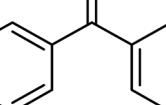
Entry	Alcohol	Product ^b	Time (h)	Yield ^c % (isolated yield%)
1			3	93 (88)
2			3	91 (86)
3			2	100 (95)
4			2.5	94 (88)
5			3	93 (88)
6			3	91 (85)
7			4	98 (91)
8			4	88 (80)
9			4	92 (84)
10			3	97 (91)
11			2	95 (86)
12			2.5	100 (96)

Table 1 (Contd.)

Entry	Alcohol	Product ^b	Time (h)	Yield ^c % (isolated yield%)
13			2.5	100 (95)
14			4.5	72 (65)
15			4	96 (87)
16			6	73 (67)

^a Reaction conditions: 1000 : 100 : 5 molar ratio for alcohol : NHPI : catalyst in CH₃CN (2 mL) under continuous stream of O₂ (5–7 mL min⁻¹) at 70 °C. ^b The products were identified by ¹H NMR spectroscopy or by comparison with the retention times of authentic samples in GC analysis. The selectivity of products were >99% based on GC analysis. ^c GC yield.

solvent amount, catalyst amount, NHPI amount and oxidant nature (Fig. 6).

Oxidation of 1-phenyl ethanol under the optimized conditions (0.5 mol% CoL₂@TiO₂ and 10 mol% NHPI at 70 °C) using a continuous stream of O₂ in acetonitrile, gave solely acetophenone in 93% yield within 3 h under visible light irradiation. CoL₂@TiO₂ exhibited high efficiency and selectivity toward aerobic oxidation of a wide range of primary and secondary benzylic alcohols under optimized conditions (Table 1). Our results revealed that, the oxidation performance affected by electronic properties of substrates. Electron-accepting groups on the phenyl rings of alcohols accelerated the reaction (Table 1, entries 3 and 4), while electron-releasing ones retarded it (Table 1, entries 9 and 10). For example, full oxidation of 4-nitro- and 4-methoxybenzyl alcohol took 2 and 4 h, respectively.

To demonstrate the chemoselectivity of the method, 2-cyclohexen-1-ol and cinnamyl alcohol as allylic alcohols were subjected to oxidation procedure. The related unsaturated carbonyl compounds were produced in high yields and the olefin moiety remained intact in both cases (Table 1, entries 13 and 16). Moreover, a molecule containing both primary benzylic hydroxyl group and sulfide group, oxidized selectively to the corresponding aldehyde in 72% yield and sulfide group which is more susceptible to oxidation was tolerated (Table 1, entry 14). Notably, no trace of ester and benzoic acid was observed resulting from over oxidation of secondary and primary alcohols, respectively. It should be mentioned that attempts to oxidize saturated aliphatic alcohols under different conditions failed.

Encouraged by the above promising results, we applied the catalytic system for oxidation of benzylic hydrocarbons.

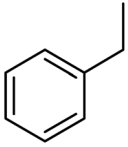
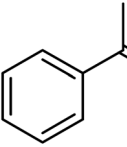
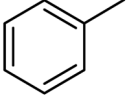
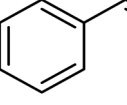
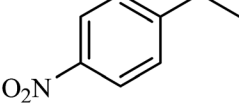
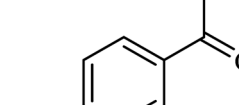
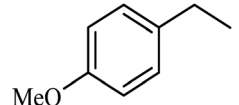
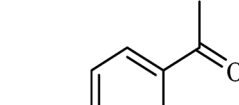
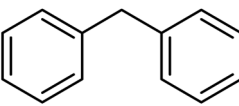
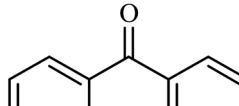
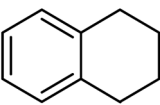
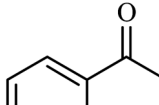
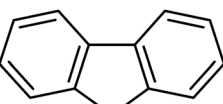
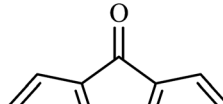
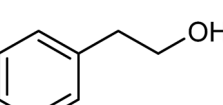
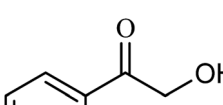
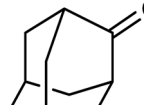
Complete transformation of ethylbenzene to acetophenone occurred within 6 h using a continuous stream of O₂ at 70 °C in the presence of 0.75 mol% CoL₂@TiO₂ nanocomposite and 10 mol% NHPI in acetonitrile under visible light irradiation. The high yields (76–97%) and excellent selectivity (>99%) to carbonyl compounds were achieved for different benzylic hydrocarbons (Table 2). A salient feature of the method is efficient and selective oxidation of toluene to benzaldehyde (Table 2, entry 2) while the formation of benzoic acid resulting from over oxidation reaction well controlled. As observed for alcohol oxidation, electron-accepting groups on the phenyl rings of benzylic hydrocarbons accelerated the reaction (Table 1, entry 3), while electron-releasing one retarded it (Table 1, entry 4). For example, 4-nitro- and 4-methoxyethylbenzene gave 95 and 86% yields of the corresponding acetophenones after 3.5 and 6.5 h, respectively. Furthermore, the catalytic system provided herein was capable of the facile oxidation of sterically hindered secondary benzylic hydrocarbons to the corresponding carbonyl compounds (Table 2, entries 5–7, 9).

The method possesses novelty regarding the chemoselectivity. 2-Phenylethanol oxidized to 2-hydroxyacetophenone while, hydroxyl group was tolerated in the reaction (Table 2, entry 8).

Table 3, summarizes the results for catalytic oxidation of various benzyl alcohols obtained under catalytic influence of CoL₂@TiO₂ nanocomposite in comparison with free CoL₂ as well as CoL₂ supported on magnetic nanoparticles (CoL₂@SMNP) in our previous report.²⁵ The results clearly highlight the superiority of title nanocatalyst in conversion rate (Table 3).

Notably, the replacement of CoL₂@TiO₂ by another nano-oxometals such as MoO₃,³¹ m-ZrO₂,³² γ-Fe₂O₃ and TiO₂, as well

Table 2 Oxidation of alkyl benzenes using NHPI/O₂ oxidative system catalyzed by CoL₂@TiO₂ nanocomposite^a

Entry	Alcohol	Product ^b	Time (h)	Yield ^c % (isolated yield%)
1			6	97 (92)
2			6	90 (84)
3			3.5	100 (95)
4			6.5	92 (86)
5			3	92 (86)
6			4	98 (92)
7			3	98 (92)
8			5.5	91 (84)
9			8	76 (71)

^a Reaction conditions: 1000 : 100 : 7.5 molar ratio for alkane : NHPI : catalyst in CH₃CN (2 mL) under O₂ (5–7 mL min⁻¹) at 70 °C. ^b The products were identified by ¹H NMR spectroscopy or by comparison with the retention times of authentic samples in GC analysis. The selectivity of products were >99% based on GC analysis. ^c GC yield.

as their nanocomposites such as CoL₂@MoO₃, CoL₂@SMNP and SMNP prolonged the oxidation of 1-phenylethanol under the same conditions (Fig. 7).

Considering the results presented in Table 3 and Fig. 7, the catalytic performance of CoL₂@TiO₂ nanocomposite can be explained on the basis of oxidation activity of Co(II) centers^{33–42}

Table 3 The comparison of catalytic activity of CoL₂@TiO₂ nanocomposite with CoL₂ and CoL₂@γ-Fe₂O₃ on the oxidation of benzylic alcohols

Entry	X	[CoL ₂] ^a	[CoL ₂] ^a @Fe ₂ O ₃ ^a	[CoL ₂] ^a @TiO ₂ ^b
		Yield ^c (%) [time (h)]	Yield ^c (%) [time (h)]	Yield ^c (%) [time (h)]
1	H	100 [14]	97 [16]	91 [3]
2	4-NO ₂	40 [14]	35 [16]	100 [2]
3	2-NO ₂	48 [14]	44 [16]	94 [2.5]
4	4-OMe	78 [14]	72 [16]	92 [4]
5	4-Cl	51 [14]	44 [16]	98 [4]
6	2-Cl	67 [14]	60 [16]	88 [4]
7	4-Me	62 [14]	57 [16]	93 [3]

^a Reaction conditions: 1000 : 100 : 5 molar ratio for alcohol : NHPI : catalyst in CH₃CN (3 mL) under continues stream of O₂ (5–7 mL min⁻¹) at 70 °C. ^b Reaction conditions: 1000 : 100 : 5 molar ratio for alcohol : NHPI : catalyst in CH₃CN (2 mL) under continues stream of O₂ (5–7 mL min⁻¹) at 70 °C. ^c GC yield.

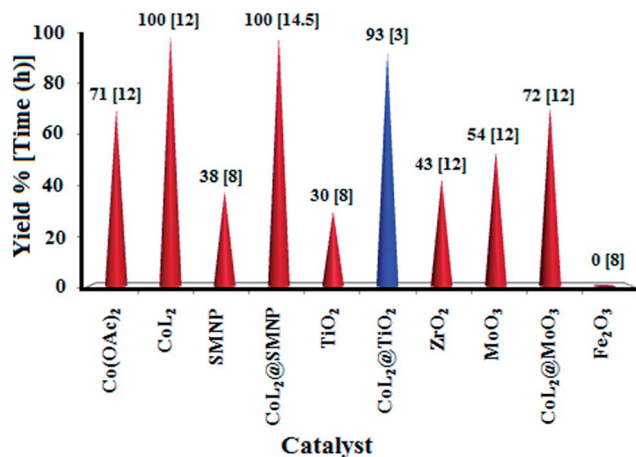


Fig. 7 The comparison of catalytic activity of CoL₂@TiO₂ nanocomposite with other nanocomposites and nanooxometals on the oxidation of 1-phenylethanol (1 mmol) in CH₃CN (2 mL) using NHPI (10 mol%) under continues stream of O₂ (5–7 mL min⁻¹) and visible light at 70 °C.

combined with photocatalytic activity of TiO₂ core which also acts as support.

To support of photocatalytic property of TiO₂ at the core of title nanocomposite, oxidation of 1-phenylethanol under UV light, visible light as well as in dark using NHPI (10 mol%) under continues stream of O₂ at 70 °C after 2 h were investigated. Accelerated reactions under light radiation particularly UV light demonstrated the photocatalytic effect of TiO₂ core on the oxidation efficiency of CoL₂@TiO₂ nanocomposite (Fig. 8).

Also, for investigation of this important issue, band gap energy values of as-prepared TiO₂, CoL₂ and CoL₂@TiO₂ were assayed. The UV-vis-DR spectra of different samples along with tangent drawn for band gap calculation are presented in Fig. 9.

The absorption threshold of pure titania at ~400 nm indicates the major light absorption in the UV region. Nevertheless,

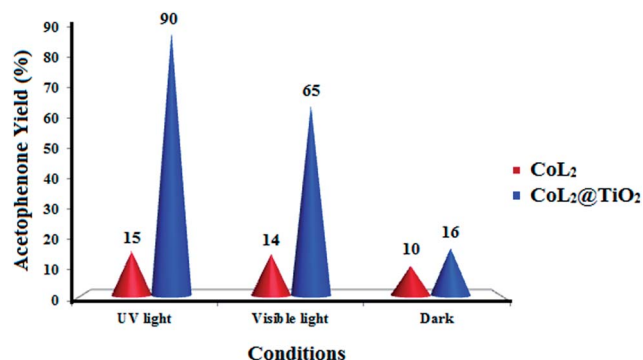


Fig. 8 The screening of photocatalytic activity of CoL₂ and CoL₂@TiO₂ nanocomposite in the oxidation of 1-phenyl ethanol using NHPI (10 mol%) under continues stream of O₂ (5–7 mL min⁻¹) at 70 °C after 2 h.

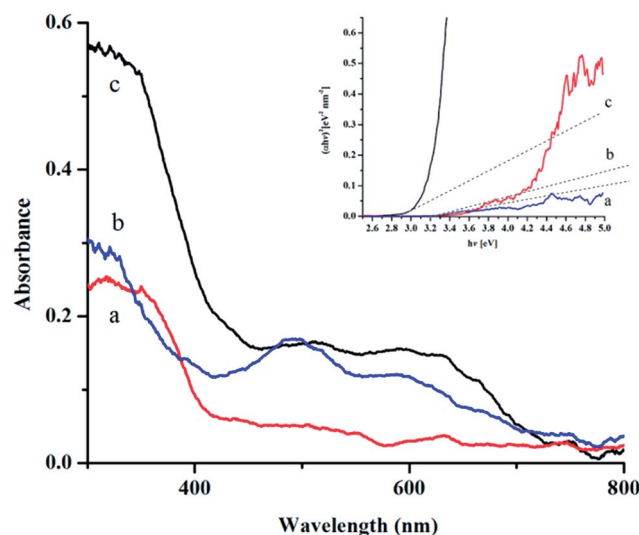


Fig. 9 Diffuse reflectance UV-vis spectra of (a) bare TiO₂ NPs, (b) CoL₂ and (c) CoL₂@TiO₂.

a red-shift of the band-edge of $\text{CoL}_2@\text{TiO}_2$ to wavelengths higher than 400 nm demonstrates higher visible light absorption than those of TiO_2 , and CoL_2 samples, making it more favorable for photocatalytic applications under visible light radiation. Diffuse reflectance UV-vis using the Kubelka–Munk formula and Tauc plot,⁴³ revealed significant reduction of the band-gap of $\text{CoL}_2@\text{TiO}_2$ nanoparticles (2.9 eV) compared with that of TiO_2 nanoparticles (3.2 eV). So, according to obtained results, a synergistic effect of cobalt Schiff base complex and TiO_2 nanoparticles can be considered for visible-light photocatalytic modification of title nanocatalyst.

The most important issues that must be resolved for heterogeneous catalysts are the lifetimes of the catalyst and the possibility that the active component can leach from the solid into solution, thereby leading to gradual deactivation of the catalyst.

The heterogeneous nature of the catalyst was confirmed in a filtration experiment. For this purpose, the catalyst was recovered by centrifuging and decantation of the reaction mixture. No catalytic activity was observed in the filtrate solution, while, aerobic oxidation of 1-phenylethanol to acetophenone proceeded well by using the recovered catalyst after that it was washed with ethylacetate and dried under vacuum (Table 1, entry 1). The ease of recovery, combined with the intrinsic

stability of the $\text{CoL}_2@\text{TiO}_2$ nanocomposite, allows the catalyst to be recovered efficiently over at least four times in aerobic C–H oxidation under conditions used in this study (Fig. 10).

The comparison of TEM images and FT-IR spectra of used $\text{CoL}_2@\text{TiO}_2$ nanocomposite (Fig. 11) with fresh one confirms that the catalyst maintains its structural integrity and size and morphology of the catalyst remained almost intact after four times recovering.

Table 4 shows the merit of this operationally simple catalytic protocol in comparison with those previously reported methods, in terms of oxygen source, conversion rate, catalyst loading and conditions used in the oxidation of benzyl alcohol as model substrate. For example, full oxidation of benzyl alcohol to benzaldehyde took only 3.5 h under O_2 in CH_3CN and using a low catalyst loading of 0.5 mol% (0.004 g).

Therefore, title methodologies are cost effective and industrially important because of using O_2 as an environmentally oxidant, visible light as energy source, reusing of an active catalyst with low catalyst loading, easy isolation of organic products. These advantages make the method amenable to scalability readily. As an example, under a semi-scaled up procedure (20.0 mmol) acetophenone was secured in 85% yield in the oxidation of 1-phenylethanol in the presence of $\text{CoL}_2@\text{TiO}_2$ nanocomposite within 3 h.

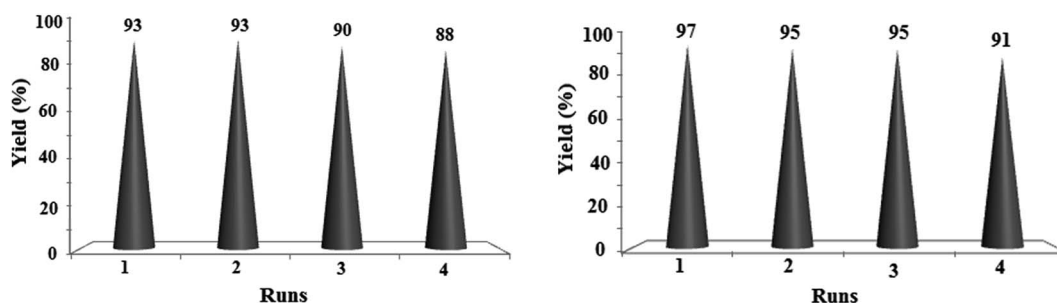


Fig. 10 Recycling of the catalytic system for oxidation of 1-phenylethanol (left) and ethylbenzene (right) under conditions used in this study.

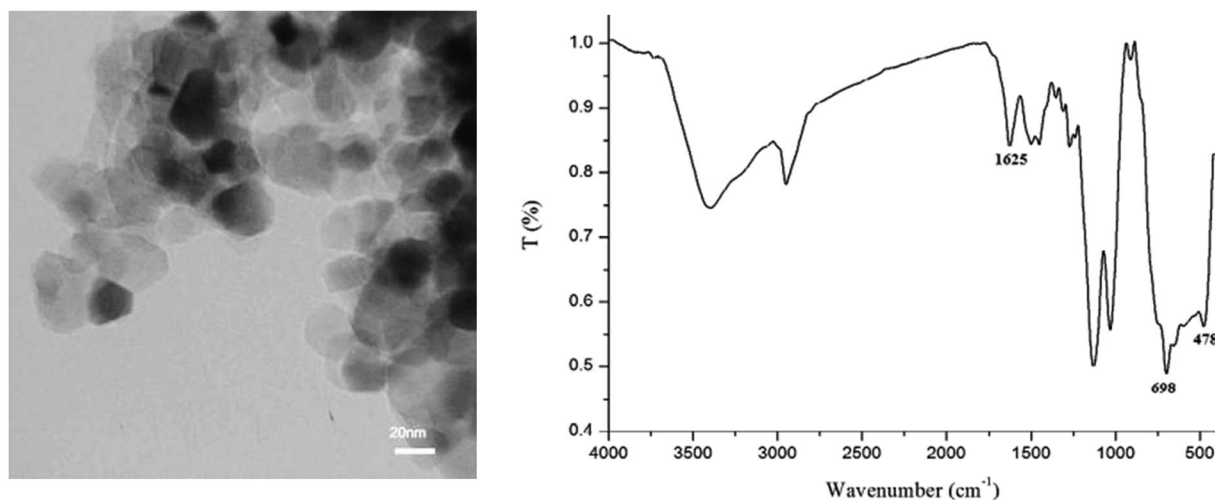


Fig. 11 The TEM image and FT-IR spectra of reused $\text{CoL}_2@\text{TiO}_2$ nanocatalyst after 4 times reuses.

Table 4 The comparison of catalytic activity of CoL₂@TiO₂ nanoparticles with other previously reported catalysts for oxidation of benzyl alcohol as model substrate

Entry	Catalyst	Catalyst amount	Conditions	Time (h)	Conversion (%)	Selectivity (%)	Ref.
1	CoL ₂ @TiO ₂	0.5 mol% (0.004 g)	MeCN/O ₂ /70 °C	3.5	91	100	^a
2	[CoL ₂ @SMNP] ^b	0.5 mol%	MeCN/O ₂ /70 °C	12	97	100	25
3	UiO-66-Sal-CuCl ₂	0.5 mmol	MeCN/O ₂ /60 °C	24	99	99	44
4	Au hollow nanospheres	5 wt%	MeOH/H ₂ O ₂ /55 °C	8	99	87	45
5	CoPc@cell ^c	0.05 g	<i>o</i> -Xylene/O ₂ /r.t.	8.5	83	100	46
6	Co(Schiff base) ₂ @SiO ₂	0.25 mol%	MeCN/O ₂ /60 °C	25	100	13	47
7	Polyaniline-supported molybdenum	22 mg	PhMe/O ₂ /100 °C	12	92	>98	48
8	Nanoshell carbon (NSC)	10 mg	1,4-Dioxane/O ₂ /70 °C	5	96	92	49
9	Pd@SBA-15	0.4 mol%	PhMe/air/80 °C	5.5	99	83	50
10	Pd@SBA-15	0.4 mol%	PhMe/O ₂ /80 °C	3.5	83	100	50
11	Co ₃ O ₄ @AC ^d	0.1 g	PhMe/O ₂ /80 °C	3	100	87.3	51
12	Ru/CNTs ^e	5.9 mol%	PhMe, H ₂ O/O ₂ /85 °C	3	98	100	52
13	AR/TiO ₂ /TEMPO	80 mg	Benzotrifluoride/O ₂ /85 °C	18	80	98	53
14	[Co(L) ₃] ^f	0.01 mmol	MeCN/TBHP/80 °C	24	51	100	54
15	RuHAP-γ-Fe ₂ O ₃ ^h	0.5 mol%	PhMe/O ₂ /90 °C	1	99	98	55
16	2,2':6',2''-Terpyridine	1 mmol	MeCN/air/r.t.	10	99	100	56
17	Co-birnessite	0.3 g mmol ⁻¹	PhMe/O ₂ /110 °C	24	84	100	57
18	[Tetrakis(<i>o</i> -chlorophenyl)porphyrinato] Co(II)	80 mg	MeCN/H ₂ O ₂ /70 °C	5	97.1	97.7	58
19	[Co(III)L' ₂] ⁱ (NO ₃) ₃ ·2CH ₃ OH	0.05 mmol	H ₂ O/H ₂ O ₂ /r.t.	8	34	85	59
20	[Co(II)L' ₂] ^j (NO ₃) ₂ ·2CH ₃ OH·H ₂ O	0.05 mmol	H ₂ O/H ₂ O ₂ /r.t.	8	94	93	59
21	Cobalt(II) complexes of amino acids-Schiff bases	0.005 mmol	H ₂ O, py/O ₂ /80 °C	4	84	100	60
22	TiO ₂	25 mg	Benzotrifluoride/O ₂ /r.t.	4	42	98	61
23	Si/Ti	25 mg	Benzotrifluoride/O ₂ /r.t.	4	46	98	61
24	Cds/TiO ₂ , <i>hv</i>	45 mg	MeCN/O ₂ /50 °C	1	65	>99	62
25	Au ₂ (DP ₆₇₃)/P25 ^k	20 mg	PhMe/O ₂ /r.t.	4	85	79	63
26	1% Pd/TiO ₂ -0.005APTES ^l	25 mg	S.F/O ₂ /120 °C	7	61.5	81.4	64
27	5% RGO-TiO ₂ ^m	8 mg	H ₂ O/O ₂ /25 °C	4	37	90	65
28	SEG-TiO ₂ ⁿ	8 mg	H ₂ O/O ₂ /25 °C	4	50	90	65

^a This work. ^b Magnetic nanoparticles (γ-Fe₂O₃, MNP) coated with starch (SMNP). ^c Cobalt(II) phthalocyanine covalently anchored to cellulose. ^d Activated carbon (AC). ^e Carbon nanotubes (CNTs). ^f Alizarin red (AR). ^g Tris-chelate complexes of cobalt(III) with *N*-[di(alkyl/aryl)carbamothioyl] benzamide derivatives. ^h Ruthenium-hydroxyapatite-encapsulated superparamagnetic γ-Fe₂O₃ nanocrystallites. ⁱ 4'-(2-Thienyl)-2,2':6',2''-ter-pyridine (L'). ^j 4'-(2-Thienyl)-2,2':6',2''-ter-pyridine (L'). ^k Au₂(DPy)/P₂₅ catalysts prepared at higher calcination temperatures (>673 K), deposition-precipitation (DP) method. ^l Aminopropyltriethoxysilane (APTES). ^m Reduced graphene oxide-TiO₂ nanocomposite (RGO). ⁿ Solvent exfoliated graphene-TiO₂ (SEG).

4. Conclusions

In conclusion, immobilizing of cobalt Schiff base complex on nanocrystalline TiO₂ improved its visible light photocatalytic properties. Our results demonstrated well the synergistic effect of cobalt Schiff base complex and TiO₂ nanoparticles on the visible-light photocatalytic activity. According to DRS analysis, the band gap energy of TiO₂ decreased significantly after functionalization with cobalt Schiff base complex. The nanocatalyst showed high oxidation stability and desired activity and selectivity in the aerobic benzylic C-H oxidation of structurally diverse set of benzylic alcohols and hydrocarbons. The additional advantage of this catalytic system is facile and efficient reusability of the solid catalyst. The use of O₂ as an environmentally friendly oxidant, visible light as a safe energy source under the influence of a reusable and durable active catalyst with low catalyst loading, along with easy isolation of organic products are the strengths of the presented work providing the scalability of the methods. Thus, our methods are cost effective which

enable the industrially important reactions to be carried out efficiently under aerobic and practically attainable conditions.

Acknowledgements

Support for this work by Research Council of University of Birjand is highly appreciated.

References

- 1 X. Lang, X. Chen and J. Zhao, *Chem. Soc. Rev.*, 2014, **43**, 473–486.
- 2 F. Cardona and C. Parmeggiani, *Transition Metal Catalysis in Aerobic Alcohol Oxidation*, Royal Society of Chemistry, 2014.
- 3 M. A. Fox and M. T. Dulay, *Chem. Rev.*, 1993, **93**, 341–357.
- 4 A. Maldotti, A. Molinari and R. Amadelli, *Chem. Rev.*, 2002, **102**, 3811–3836.
- 5 G. Palmisano, V. Augugliaro, M. Pagliaro and L. Palmisano, *Chem. Commun.*, 2007, 3425–3437.

- 6 M. Fagnoni, D. Dondi, D. Ravelli and A. Albini, *Chem. Rev.*, 2007, **107**, 2725–2756.
- 7 Y. Shiraishi and T. Hirai, *J. Photochem. Photobiol., C*, 2008, **9**, 157–170.
- 8 F. Amano, O.-O. Prieto-Mahaney, Y. Terada, T. Yasumoto, T. Shibayama and B. Ohtani, *Chem. Mater.*, 2009, **21**, 2601–2603.
- 9 X. Han, X. Wang, S. Xie, Q. Kuang, J. Ouyang, Z. Xie and L. Zheng, *RSC Adv.*, 2012, **2**, 3251–3253.
- 10 J. M. d. S. e. Silva, M. Pastorello, M. Strauss, C. M. Maroneze, F. A. Sigoli, Y. Gushikem and I. O. Mazali, *RSC Adv.*, 2012, **2**, 5390–5397.
- 11 S. Bingham and W. A. Daoud, *J. Mater. Chem.*, 2011, **21**, 2041–2050.
- 12 R. Asahi, T. Morikawa, T. Ohwaki, K. Aoki and Y. Taga, *Science*, 2001, **293**, 269–271.
- 13 J. Virkutyte and R. S. Varma, *RSC Adv.*, 2012, **2**, 1533–1539.
- 14 S. Sakthivel, M. Shankar, M. Palanichamy, B. Arabindoo, D. Bahnemann and V. Murugesan, *Water Res.*, 2004, **38**, 3001–3008.
- 15 S. Ko, C. K. Banerjee and J. Sankar, *Composites, Part B*, 2011, **42**, 579–583.
- 16 M. Murdoch, G. Waterhouse, M. Nadeem, J. Metson, M. Keane, R. Howe, J. Llorca and H. Idriss, *Nat. Chem.*, 2011, **3**, 489–492.
- 17 W. M. Campbell, K. W. Jolley, P. Wagner, K. Wagner, P. J. Walsh, K. C. Gordon, L. Schmidt-Mende, M. K. Nazeeruddin, Q. Wang and M. Grätzel, *J. Phys. Chem. C*, 2007, **111**, 11760–11762.
- 18 W. Zhao, Y. Sun and F. N. Castellano, *J. Am. Chem. Soc.*, 2008, **130**, 12566–12567.
- 19 M. Nieto-Suárez, G. Palmisano, M. L. Ferrer, M. C. Gutiérrez, S. Yurdakal, V. Augugliaro, M. Pagliaro and F. del Monte, *J. Mater. Chem.*, 2009, **19**, 2070–2075.
- 20 J. Yu, L. Zhang, B. Cheng and Y. Su, *J. Phys. Chem. C*, 2007, **111**, 10582–10589.
- 21 H. Zhou, T. Fan and D. Zhang, *ChemCatChem*, 2011, **3**, 513–528.
- 22 H. Zhou, X. Li, T. Fan, F. E. Osterloh, J. Ding, E. M. Sabio, D. Zhang and Q. Guo, *Adv. Mater.*, 2010, **22**, 951–956.
- 23 J. Sarkar, V. T. John, J. He, C. Brooks, D. Gandhi, A. Nunes, G. Ramanath and A. Bose, *Chem. Mater.*, 2008, **20**, 5301–5306.
- 24 X. Chen and S. S. Mao, *Chem. Rev.*, 2007, **107**, 2891–2959.
- 25 M. Jafarpour, A. Rezaeifard, V. Yasinzadeh and H. Kargar, *RSC Adv.*, 2015, **5**, 38460–38469.
- 26 M. Jafarpour, M. Ghahramaninezhad and A. Rezaeifard, *New J. Chem.*, 2014, **38**, 2917–2926.
- 27 S. Naik, A. Salker, S. Yusuf and S. Meena, *J. Alloys Compd.*, 2013, **566**, 54–61.
- 28 X. Wang, Y. Zhang, H. Meng, Z. Wang and Z. Zhang, *J. Alloys Compd.*, 2011, **509**, 7803–7807.
- 29 W. Wang, H. Yang, T. Xian and J. Jiang, *Mater. Trans.*, 2012, **53**, 1586–1589.
- 30 R. S. Gaikwad, S.-Y. Chae, R. S. Mane, S.-H. Han and O.-S. Joo, *Int. J. Electrochem.*, 2011, **2011**, 729141.
- 31 M. Jafarpour, A. Rezaeifard, M. Ghahramaninezhad and T. Tabibi, *New J. Chem.*, 2013, **37**, 2087–2095.
- 32 M. Jafarpour, E. Rezapour, M. Ghahramaninezhad and A. Rezaeifard, *New J. Chem.*, 2014, **38**, 676–682.
- 33 Y. Yoshino, Y. Hayashi, T. Iwahama, S. Sakaguchi and Y. Ishii, *J. Org. Chem.*, 1997, **62**, 6810–6813.
- 34 C. Parmeggiani and F. Cardona, *Green Chem.*, 2012, **14**, 547–564.
- 35 Y. Ishii and S. Sakaguchi, *Catal. Today*, 2006, **117**, 105–113.
- 36 H. Ma, J. Xu, Q. Zhang, H. Miao and W. Wu, *Catal. Commun.*, 2007, **8**, 27–30.
- 37 D. Habibi, A. Faraji, M. Arshadi, S. Heydari and A. Gil, *Appl. Catal., A*, 2013, **466**, 282–292.
- 38 T. Iwahama, S. Sakaguchi, Y. Nishiyama and Y. Ishii, *Tetrahedron Lett.*, 1995, **36**, 6923–6926.
- 39 T. Iwahama, Y. Yoshino, T. Keitoku, S. Sakaguchi and Y. Ishii, *J. Org. Chem.*, 2000, **65**, 6502–6507.
- 40 S. J. S. Kalra, T. Punniyamurthy and J. Iqbal, *Tetrahedron Lett.*, 1994, **35**, 4847–4850.
- 41 A. K. Mandal and J. Iqbal, *Tetrahedron*, 1997, **53**, 7641–7648.
- 42 V. B. Sharma, S. L. Jain and B. Sain, *J. Mol. Catal. A: Chem.*, 2004, **212**, 55–59.
- 43 A. T. Kuvarega, R. W. Krause and B. B. Mamba, *J. Phys. Chem. C*, 2011, **115**, 22110–22120.
- 44 J. Hou, Y. Luan, J. Tang, A. M. Wensley, M. Yang and Y. Lu, *J. Mol. Catal. A: Chem.*, 2015, **407**, 53–59.
- 45 M. Sasidharan, S. Anandhakumar, P. Bhanja and A. Bhaumik, *J. Mol. Catal. A: Chem.*, 2016, **411**, 87–94.
- 46 A. Shaabani, S. Keshipour, M. Hamidzad and S. Shaabani, *J. Mol. Catal. A: Chem.*, 2014, **395**, 494–499.
- 47 F. Rajabi and B. Karimi, *J. Mol. Catal. A: Chem.*, 2005, **232**, 95–99.
- 48 S. Velusamy, M. Ahamed and T. Punniyamurthy, *Org. Lett.*, 2004, **6**, 4821–4824.
- 49 Y. Kuang, N. M. Islam, Y. Nabae, T. Hayakawa and M. a. Kakimoto, *Angew. Chem., Int. Ed.*, 2010, **49**, 436–440.
- 50 B. Karimi, S. Abedi, J. H. Clark and V. Budarin, *Angew. Chem., Int. Ed.*, 2006, **45**, 4776–4779.
- 51 J. Zhu, K. Kailasam, A. Fischer and A. Thomas, *ACS Catal.*, 2011, **1**, 342–347.
- 52 X. Yang, X. Wang and J. Qiu, *Appl. Catal., A*, 2010, **382**, 131–137.
- 53 M. Zhang, C. Chen, W. Ma and J. Zhao, *Angew. Chem., Int. Ed.*, 2008, **120**, 9876–9879.
- 54 N. Gunasekaran, P. Jerome, S. W. Ng, E. R. T. Tiekink and R. Karvembu, *J. Mol. Catal. A: Chem.*, 2012, **353–354**, 156–162.
- 55 K. Mori, S. Kanai, T. Hara, T. Mizugaki, K. Ebitani, K. Jitsukawa and K. Kaneda, *Chem. Mater.*, 2007, **19**, 1249–1256.
- 56 Z. Yin, G. Zhang, T. Phoenix, S. Zheng and J. C. Fettinger, *RSC Adv.*, 2015, **5**, 36156–36166.
- 57 A. Kamimura, Y. Nozaki, M. Nishiyama and M. Nakayama, *RSC Adv.*, 2013, **3**, 468–472.
- 58 F. Adam and W.-T. Ooi, *Appl. Catal., A*, 2012, **445**, 252–260.
- 59 A. N. Kharat, A. Bakhoda and B. T. Jahromi, *Polyhedron*, 2011, **30**, 2768–2775.

- 60 S. M. Seyedi, R. Sandaroos and G. H. Zohuri, *Chin. Chem. Lett.*, 2010, **21**, 1303–1306.
- 61 Q. Wang, M. Zhang, C. Chen, W. Ma and J. Zhao, *Angew. Chem., Int. Ed.*, 2010, **49**, 7976–7979.
- 62 I. Tamiolakis, I. N. Lykakis and G. S. Armatas, *Catal. Today*, 2015, **250**, 180–186.
- 63 D. Tsukamoto, Y. Shiraishi, Y. Sugano, S. Ichikawa, S. Tanaka and T. Hirai, *J. Am. Chem. Soc.*, 2012, **134**, 6309–6315.
- 64 P. Weerachawanasak, G. J. Hutchings, J. K. Edwards, S. A. Kondrat, P. J. Miedziak, P. Prasertham and J. Panpranot, *Catal. Today*, 2015, **250**, 218–225.
- 65 L. Yuan, Q. Yu, Y. Zhang and Y.-J. Xu, *RSC Adv.*, 2014, **4**, 15264–15270.